JOURNAL OF Materials CHEMISTRY

Preparation, characterization and photochemical properties of ordered macroporous hybrid silica materials based on monovacant Keggin-type polyoxometalates

Yihang Guo,[a] Yu Yang,[a] Changwen Hu,*[a] Caixin Guo,[a] Enbo Wang,[a] Yongcun Zou[b] and Shouhua Feng[b]

[a]*Institute of Polyoxometalate Chemistry, Faculty of Chemistry, Northeast Normal University, Changchun 130024, P. R. China. E-mail: huchw@nenu.edu.cn*
[b]*State Key Laboratory of Inorganic Synthesis and Preparative Chemistry, Jilin University, Changchun 130023, P. R. China*

Received 27th November 2001, Accepted 25th June 2002
First published as an Advance Article on the web 9th August 2002

High loading, three-dimensionally ordered macroporous (3DOM) hybrid silica materials based on monovacant Keggin-type polyoxometalates (POMs) $[X^{n+}W_{11}O_{39}]^{(12-n)-}$ (XW_{11}; X^{n+} = P^{5+}, Si^{4+}, Ge^{4+}, B^{3+}) were prepared *via* sol–gel as well as templating techniques. XW_{11} clusters were incorporated into the wall structures of macroporous silica, resulting in hybrid XW_{11}–SiO_2 composites. Formation of the hybrid materials was due to the chemical grafting of organosilanol groups from the silica network onto the surface oxygen atoms at vacant sites on the XW_{11} clusters. The products were characterized by UV diffuse reflectance spectra (UV/DRS), infrared (IR) spectra, ^{29}Si and ^{31}P MAS NMR, inductively coupled plasma atomic emission spectrometry (ICP-AES), scanning electron microscopy (SEM), transmission electron microscopy (TEM) and nitrogen adsorption isotherms. The study indicates that the primary Keggin structures remain intact in the hybrid materials, and that the products demonstrate three-dimensionally ordered macropores with pore diameters in the range of 285 to 385 nm. The composites exhibited photocatalytic activity to degrade aqueous malic acid (MA) under irradiation in the near-UV region; leakage of XW_{11} from the hybrid materials was hardly observed during catalytic tests.

1 Introduction

Ordered macroporous materials with pore sizes in the submicrometer range have elicited much interest recently because of their applications in catalysis, separation processes and photonic crystals with tunable band gaps.[1–7] Among the wide range of preparative methods for macroporous materials, templating methods can provide macroporous solids with narrow macropore size distributions and relatively high porosity.[8] In the case of this method, the templates used are mainly polymer gels,[9] emulsions,[10] latex spheres,[11] and even bacteria.[12] By using latex sphere templates, macroporous materials with three-dimensionally ordered arrays such as macroporous oxides (oxides of Si, Ti, Zr, Al, Sb, W, Fe and mixtures of these), silicates, aluminophosphates, hybrid organosilicates and polymers (polyacrylamide and polyurethane) have been prepared.[13–16] These products are obtained by filling the voids between a close-packed array of polystyrene (PS) or silica spheres with a precursor fluid that forms a solid skeleton around spheres. Template removal is achieved by either calcination or extraction, leading to solid materials with macropores (diameters of tens to hundreds of nanometers).[17–20]

The photochemical, electrochromic and magnetic properties of POMs are now leading to increased interest in materials with these properties.[21,22] The recent synthesis of new hybrid organic–inorganic materials *via* covalent binding of electrophilic organic moieties to nucleophilic surface oxygen atoms in lacunary POMs is particularly attractive because the resulting advanced materials must exhibit specific properties.[23–29] In this kind of composite, lacunary POMs such as tri-, di-, and monovacant Keggin anions were selected as the inorganic precursors, and they exhibited reactivity towards the electrophilic organic groups such as RSi^{3+}, RPO^{2+} and RSn^{3+}. Therefore, the hybrids based on lacunary Keggin units were formed *via* Y–O–W bridges (Y = Si, P, Sn).

In the present work, we have prepared four kinds of ordered macroporous hybrid silica materials based on lacunary POMs. Monovacant Keggin units XW_{11} (X = P, Si, Ge, B) were chosen for these preparations, due to their reactivity toward silanol groups. At first, tetraethoxysilane (TEOS) was reacted with XW_{11} under acidic conditions, followed by condensation around PS colloidal crystals. Subsequently, the PS template was removed from the materials by refluxing in a tetrahydrofuran (THF)/acetone solution. The products were characterized by UV/DRS, IR, ^{29}Si and ^{31}P MAS NMR, ICP-AES, SEM, TEM and nitrogen adsorption determination which indicated that the syntheses produced ordered macroporous silica materials with high loadings of XW_{11} incorporated throughout the wall structures, and that the primary Keggin structures remained intact in the hybrid materials. The photocatalytic activity of the composites was studied *via* degradation of aqueous MA. MA is a model molecule for partially oxidized products found in either biomass or in various degradative processes.

2 Experimental

2.1 Materials

Monodisperse polystyrene latex spheres were synthesized in an emulsifier-free emulsion process.[2] Closed-packing arrays of latex spheres were formed on constant stirring of the suspension at *ca.* 260 rpm and subsequent slow centrifugation at *ca.* 800 rpm, then allowed to air-dry. The resulting latex spheres were extremely uniform and their average diameter is *ca.* 500 nm, estimated using SEM (Fig. 1A).

 DOI: 10.1039/b110873p

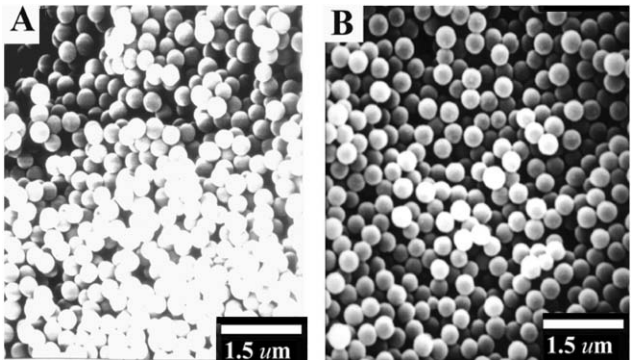

Fig. 1 SEM image of (A) monodisperse PS latex spheres, and (B) PS latex spheres coated with SiW_{11}–SiO_2.

Table 1 Main relevant mid-IR data (cm^{-1}) of the starting XW_{11} and their corresponding hybrid silica materials

Sample	ν_{as}(X–O)[a]	ν_{as}(W=O_{ter})	ν_{as}(W–O–W)
PW_{11}	1095, 1043	953	862, 833, 805
PW_{11}–SiO_2	1079[b]	953	870, 797, 672
SiW_{11}	995	950	882, 796, 728
SiW_{11}–SiO_2	1081[c]	962	804, 697, 626
GeW_{11}	959	882	796, 697, 659
GeW_{11}–SiO_2	956	881	792, 733, 676
BW_{11}	958	877	821, 744, 668
BW_{11}–SiO_2	961	908	820, 750, 673

[a]X = P, Si, Ge, B, respectively. [b]This vibration band may also originate from Si–O–Si in the silica framework. [c]The vibration peak of Si–O in the central SiO_4 unit of SiW_{11} in the hybrid macroporous silica materials was totally covered by an intense broad peak due to Si–O–Si in the silica framework at 1080 cm^{-1}, therefore, the data may originate from a combination of silica and SiW_{11} or γ-SiW_{10} together.

The following reagents are from commercial sources (China) and were used as received (analytical reagent grade). $Na_2WO_4{\cdot}2H_2O$, Na_2HPO_4, H_3BO_3, $Na_2SiO_3{\cdot}9H_2O$, K_2CO_3, GeO_2, $K_2S_2O_8$, styrene, ethanol (EtOH), TEOS, THF and acetone. Doubly distilled water was used in all experiments.

Preparations of $Na_7PW_{11}O_{39}$, $K_6Na_2SiW_{11}O_{39}$, $K_6Na_2GeW_{11}O_{39}$ and $K_6NaHBW_{11}O_{39}$ were adapted from literature methods.[30,31] IR data for the products are shown in Table 1. Elemental analysis for $Na_7PW_{11}O_{39}$ (found): P, 1.01; W, 63.9; Na, 5.26%. Elemental analysis for $K_6Na_2SiW_{11}O_{39}$: Si, 0.88; W, 62.6; K, 7.35; Na, 1.44%. Elemental analysis for $K_6Na_2GeW_{11}O_{39}$: Ge, 2.21; W, 62.8; Na, 1.41; K, 7.15%; Elemental analysis for $K_6NaHBW_{11}O_{39}$: B, 0.32; W, 63.1; Na, 0.68; K, 6.91%.

2.2 Preparation of macroporous XW_{11}–SiO_2 hybrid materials

The experimental conditions for the preparation of XW_{11}–SiO_2 materials are summarized in Table 2, and the procedure is described below. XW_{11} (2.1 g) was dissolved in water at room temperature, and a small amount of 4 M HNO_3 was added dropwise to the above solution under vigorous stirring; note: the pH of the solution should not be lower than 4. EtOH and TEOS were mixed in another container, and the mixture was acidified with a small amount of 4 M HNO_3. The acidic TEOS was added to the aqueous XW_{11} solution with vigorous stirring, and the pH of the resulting mixture was adjusted to *ca.* 2.0 to 3.3 for the different precursors used (see Table 2). The reaction solution was stirred for 10 to 90 min, respectively, until homogeneous silica sol functionalized with XW_{11} was obtained. The clear sol obtained was then added dropwise to PS spheres deposited on filter paper in a Büchner funnel while suction was applied, and the sol should cover the PS spheres completely. The coated PS latex spheres (XW_{11}–SiO_2–PS) were dried in a vacuum for 24 h at room temperature. The dried XW_{11}–SiO_2–PS (4 g) was dispersed into a THF/acetone (15 ml for each) solution, and then refluxed for 5 days. Thus, most of the PS template was removed from the materials. The white XW_{11}–SiO_2 powder was recovered by centrifugation and washed with THF/acetone, then acetone. The yield of the products was *ca.* 50%.

Table 2 Experimental conditions for the preparation of XW_{11}–SiO_2 hybrid materials

Inorganic precursor	Molar ratio TEOS : POM : H_2O : EtOH	Hydrolysis time/min	pH[a]	Product
PW_{11}	30 : 1 : 333 : 133	10	2.2 ± 0.2	PW_{11}–SiO_2
SiW_{11}	30 : 1 : 397 : 133	30	2.5 ± 0.2	SiW_{11}–SiO_2
GeW_{11}	30 : 1 : 463 : 133	60	3.0 ± 0.3	GeW_{11}–SiO_2
BW_{11}	30 : 1 : 1389 : 133	90	3.0 ± 0.3	BW_{11}–SiO_2

[a]Acidity of the mixture of acidic TEOS and aqueous XW_{11} solution.

Elemental analysis for SiW_{11}–SiO_2 (loading on the composite): W, 20.5; SW_{11}, 32.7%. Si loading in the SW_{11}–SiO_2 composite could not be determined accurately because the sample was digested with HF/HNO_3 before ICP-AES determination. Elemental analysis for PW_{11}–SiO_2: P, 0.38; W, 24.7; PW_{11}, 38.6%. Elemental analysis for GeW_{11}–SiO_2: Ge, 0.61; W, 16.8; GeW_{11}, 26.8%. Elemental analysis for BW_{11}–SiO_2: B, 0.046; W, 8.60; BW_{11}, 13.6%.

2.3 Characterization

Elemental analysis was performed on a Leeman Plasma Spec (I) ICP-AES. UV/DRS and IR spectra were recorded on a Shimadzu UV-2201 UV-VIS spectrophotometer and a Nicolet Magna 560 IR spectrophotometer, respectively. Samples for UV/DRS were prepared by diluting the white powders with $BaSO_4$. Samples for the mid-IR range were obtained in the form of KBr pellets, and samples for the far-IR range were obtained in the form of polyethylene films. ^{29}Si and ^{31}P MAS NMR spectra were obtained on a Varian Unity-400 NMR spectrometer. SEM micrographs were obtained on a Hitachi S-570 scanning electron microscope, and TEM micrographs were obtained on a Hitachi H-600 transmission electron microcsope. BET specific surface areas were calculated from the nitrogen adsorption isotherm determined at −196 °C using an ASAP 2010M surface analyzer (the samples were outgassed under vacuum at 200 °C).

2.4 Photocatalytic testing

The photoreactor was designed with a cylindrical quartz cell configuration and an internal light source surrounded by a quartz jacket, where the suspension of the catalyst and an aqueous MA completely surrounded the light source. The temperature of the suspension was maintained at 20 ± 2 °C by circulation of water through an external cooling coil. The optical pathlength was *ca.* 2 cm. The light source was a 125 W high-pressure mercury lamp (abbreviated HPML, output mainly at 313.2 nm).[32,33]

The general photocatalytic procedure was carried out as follows. The catalyst (containing 50 mg of pure XW_{11} in each XW_{11}–SiO_2 composite) was suspended in a fresh aqueous MA solution (100 mg l^{-1}). The suspension (70 ml) was ultrasonicated for 10 min and stirred in the dark for 30 min to obtain a good dispersion. The lamp was inserted into the suspension after its intensity became stable. The suspension was vigorously stirred during the process. All degradation experiments were carried out at 20 ± 2 °C with the photoreactor open to air.

After the reaction finished, XW_{11}–SiO_2 suspensions were centrifuged. Decreases in the MA concentrations and changes

in the concentrations of the intermediates (mainly acetic acid and formic acid) were analyzed simultaneously using a DX-300 ion chromatograph (IC) equipped with a conductivity detector and an ICE-ASI anion column. Some of the intermediates were identified by a HP 6890 GC/ 5973 MS equipped with a HP-5 column.

3 Results and discussion

3.1 Preparation of macroporous XW_{11}–SiO_2 hybrid materials

In order to obtain hybrid macroporous silica materials with periodic pore structures, it is critical to prepare a uniformly sized PS template. The SEM graph (Fig. 1A) shows that the PS spheres prepared in the present work were monodisperse and well distributed, and the average size of PS spheres was *ca.* 500 nm.

Inorganic precursor XW_{11} was introduced into the PS template in the form of a hybrid silica sol. Hybrid XW_{11}–SiO_2 materials were formed due to the following two facts. First, the 1 : 11 series of polyoxotungstates, XW_{11}, are the monovacant lacunary derivatives of the Keggin anions $[X^{n+}W_{12}O_{40}]^{(8-n)-}$. As removal of a tungsten–oxygen octahedral moiety from a saturated polyoxotungstate framework leads to an increase and localization of the anionic charge, the resulting lacunary anion becomes highly nucleophilic and reacts easily with electrophilic groups. Second, hydrolysis of an organosiloxane such as $Si(OC_2H_5)_4$ under acidic conditions can yield organosilanol containing products such as $Si(OSi)_3(OH)$ (Q^3), $Si(OSi)_2(OH)_2$ (Q^2), and $Si(OSi)(OH)_3$ (Q^1), as well as the final hydrolysis product $Si(OSi)_4$ (Q^4). The above products form a silica network with electrophilic surface silicon atoms in the surface silanol groups, ≡Si–OH, which demonstrate chemical reactivity toward lacunary POMs. Therefore, the XW_{11}–SiO_2 hybrid materials formed through grafting of silanol groups onto the surface of XW_{11}. Formation of the latex-templated precursor XW_{11}–SiO_2–PS was achieved by permeating the hybrid XW_{11}–SiO_2 sol into the voids of PS spheres during the vacuum-assisted percolation process. The structure of XW_{11}–SiO_2–PS was cemented *via* evaporation of water during drying of the XW_{11}–SiO_2–PS at room temperature, which resulted in the particulate gel around the ordered PS lattice. The SEM image of the XW_{11}–SiO_2–PS particulate is shown in Fig. 1B, indicating that the voids of PS spheres are filled with the XW_{11}–SiO_2 composites. However, we do not observe whether individual spheres are coated with the composite.

During the process of preparation of the hybrid silica materials, two requirements should be satisfied. First, the inorganic precursor should have a high solubility in water in order to avoid collapse of the XW_{11}–SiO_2 wall. On the other hand, the high water solubility of XW_{11} often results in relatively high XW_{11} loading in the product. Among four XW_{11} compounds selected in the present work, PW_{11} (sodium salt) has the highest water solubility, therefore, PW_{11} loading on the silica support is the highest (38.6%), and the PW_{11}–SiO_2 wall is relatively thick (90 ± 10 nm; see Table 3). As for BW_{11}, its low water-solubility resulted in the lowest loading (13.6%) because it was greatly diluted during the process of preparation of the BW_{11}–SiO_2 sol. Second, in order to avoid conversion of 1 : 11 complexes to 1 : 12 complexes during the course of TEOS hydrolysis, the pH of the acidification of XW_{11} should be higher than 4, and the pH of the mixture of TEOS and aqueous XW_{11} should be higher than 2. Under this acidity, homogeneous sol was achieved by increasing the hydrolysis time of TEOS. The hydrolysis time was different for the different inorganic precursors used (see Table 2), *e.g.*, when PW_{11} was used as the precursor, the time was the shortest (10 min); as for BW_{11}, the time was the longest (90 min). However, too long a hydrolysis time produced a high viscosity sol which only poorly percolated into the voids of the spheres resulting in non-porous materials (confirmed by SEM).

Removal of the PS template from XW_{11}–SiO_2–PS led to 3DOM materials. Considering that thermal decomposition of the POMs begins at *ca.* 350 °C,[34] we selected extraction but not calcination as the best method to remove PS from the composites. After refluxing the XW_{11}–SiO_2–PS composites in a THF/acetone solution for 5 days, most of the PS spheres were removed (confirmed by IR spectra), and the porous materials were formed (Fig. 2) with XW_{11}–SiO_2 forming the wall structure.

Table 3 Wall thickness, macropore diameter and BET surface areas of XW_{11}–SiO_2 materials

Sample	Wall thickness/nm	Macropore diameter/nm	BET surface area/m^2 g^{-1}
BW_{11}–SiO_2	60 ± 10	350 ± 50	91.8
SiW_{11}–SiO_2	65 ± 10	350 ± 50	98.9
GeW_{11}–SiO_2	70 ± 10	320 ± 50	25.8
PW_{11}–SiO_2	90 ± 10	320 ± 50	81.0

3.2 Characterization of the macroporous XW_{11}–SiO_2 hybrid materials

The four XW_{11}–SiO_2 (X = B, Ge, P, Si) composites all exhibit UV absorption maxima at 200–206 nm and 260–268 nm (Fig. 3). By comparison with the starting Keggin units, XW_{11}, these bands are attributed to oxygen-to-tungsten charge-transfer (O → W CT) at W=O and W–O–W bonds, respectively. Generally, the UV absorption peak arising from W–O–W bonds is flat for monovacant Keggin units and sharp for saturated Keggin units. Therefore, from Fig. 3 we tentatively infer that the Keggin units in the XW_{11}–SiO_2 composites are still in the lacunary structure, particularly for the PW_{11}–SiO_2 and SiW_{11}–SiO_2 composites.

Pure XW_{11} compounds display a characteristic infrared fingerprint in the region from *ca.* 1100 to 700 cm^{-1},[34] attributed to X–O (X = P, B, Ge, Si) in the central XO_4 unit, W=O and W–O–W vibrations of XW_{11}. These characteristic IR

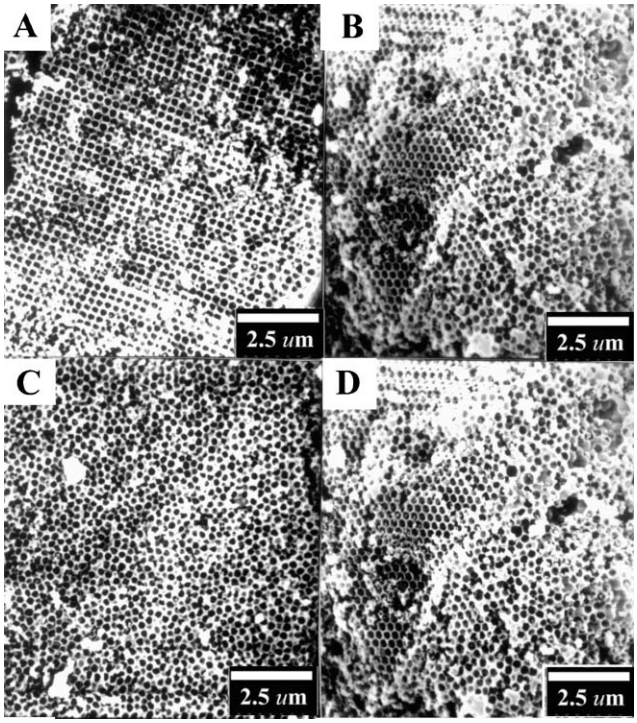

Fig. 2 SEM images of the macroporous hybrid silica materials based on XW_{11}. (A) PW_{11}–SiO_2, (B) SiW_{11}–SiO_2, (C) GeW_{11}–SiO_2, (D) BW_{11}–SiO_2.

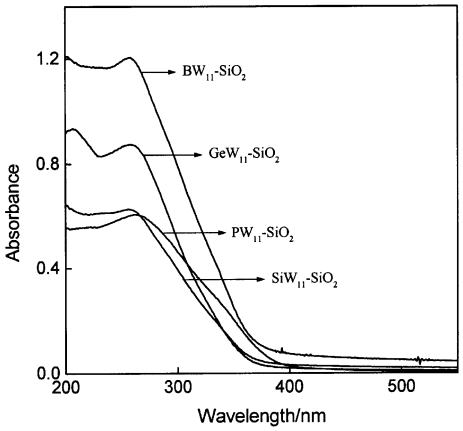

Fig. 3 UV/DRS for the macroporous hybrid silica materials based on XW_{11}.

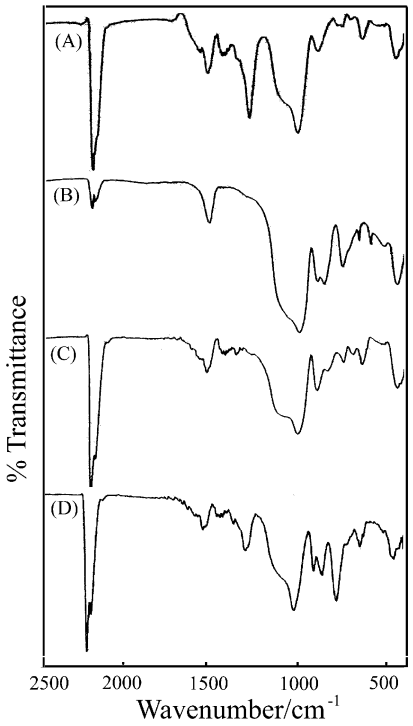

Fig. 4 Mid-IR spectra of (A) PW_{11}–SiO_2, (B) SiW_{11}–SiO_2, (C) GeW_{11}–SiO_2, and (D) BW_{11}–SiO_2 composite in a KBr matrix.

absorption data are very useful to identify the structures of XW_{11}. From Table 1 it can be seen that GeW_{11}–SiO_2 and BW_{11}–SiO_2 (Fig. 4) have similar vibration bands to those of the corresponding pure GeW_{11} and BW_{11}, respectively, suggesting that the primary GeW_{11} or BW_{11} structure remained intact regardless of the functionality of the polyanions. It is also observed that the stretching vibrational bands at W–O–W bonds (ν(W–O–W)) are shifted to higher frequency compared with those of the starting GeW_{11} or BW_{11}. The IR absorbance band at 1080 cm^{-1} is due to Si–O–Si vibration in the silica framework. In the case of SiW_{11}–SiO_2, this intense and broad Si–O–Si vibration band covered the Si–O vibration band from the central SiO_4 unit of SiW_{11}. Therefore, based on the peaks appearing at the mid-IR region, we can hardly confirm that the structural integrity of SiW_{11} has been preserved after formation of the SiW_{11}–SiO_2 hybrid materials. However, the vibrational bands of SiW_{11}–SiO_2 at W=O_{ter} bonds still maintain the main characteristic of SiW_{11} but not SiW_{12}, *e.g.*,

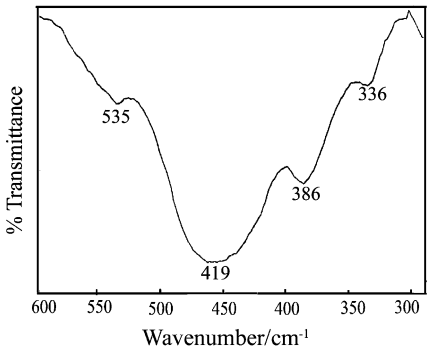

Fig. 5 Far-IR spectrum of SiW_{11}–SiO_2 composite in a polyethylene film.

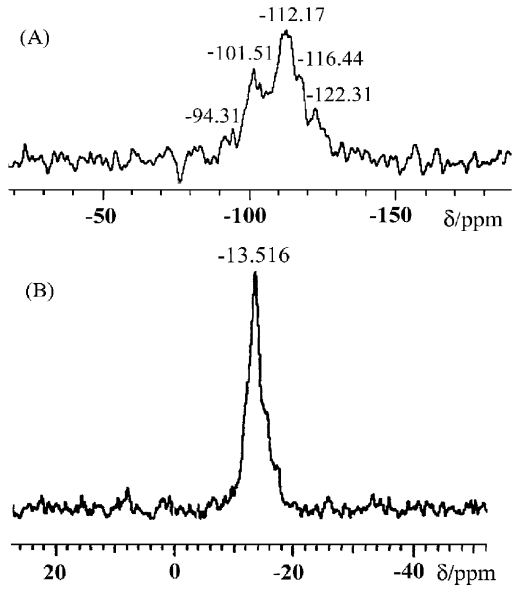

Fig. 6 (A) ^{29}Si MAS NMR spectrum of SiW_{11}–SiO_2, and (B) ^{31}P MAS NMR spectrum of PW_{11}–SiO_2.

determined ν_{as}(W=O_{ter}) for SiW_{11}, SiW_{12}, and SiW_{11}–SiO_2 were 950, 988.6, and 962 cm^{-1}, respectively.

Far-IR spectra (Fig. 5) and ^{29}Si MAS NMR (Fig. 6A) support the presence of an Si–O bond from the central SiO_4 of SiW_{11} in SiW_{11}–SiO_2. First, the deformation band of SiW_{11}–SiO_2 at 535 cm^{-1} is in agreement with the starting SiW_{11} (538 cm^{-1}), attributed to a deformation vibration of an Si–O bond from the central SiO_4 of SW_{11} (δ(Si–O)). It was also observed that the deformation bands at W–O–W bonds (δ(W–O–W)) were shifted to higher frequencies as compared with pure SiW_{11} (354 and 318 cm^{-1} respectively). Second, the ^{29}Si MAS NMR spectrum of SiW_{11}–SiO_2 indicates that the resonance at δ −94.3 ppm originated from the central SiO_4 unit of the SiW_{11} cluster, similar to that of the parent SiW_{11} (δ −93.0 ppm), suggesting that the Si–O bond in the central SiO_4 of SiW_{11} is also present in the hybrid materials. The rest of the resonances originated from Q^4 (−122.31 ppm), Q^3 (−116.44 ppm), Q^2 (−112.17 ppm), and Q^1 (−101.51 ppm), indicating that the surface silanol groups existed in the hybrid materials. Pure PW_{11} has two stretching vibrational bands for the P–O bond in the central PO_4 unit, *i.e.*, 1095 and 1043 cm^{-1}, but only one stretching vibrational band, at 1079 cm^{-1}, was observed for PW_{11}–SiO_2. The vibrational bands at W=O_{ter} bonds still maintain the main characteristics of PW_{11} but not PW_{12}, *e.g.*, determined ν_{as}(W=O_{ter}) for PW_{11}, PW_{12}, and PW_{11}–SiO_2 are 953, 983, and 953 cm^{-1}, respectively. In addition, the ^{31}P MAS

NMR spectrum showed that the chemical shift of the PW_{11}–SiO_2 composite appeared at −13.5 ppm (Fig. 6B). Determined ^{31}P chemical shifts for pure saturated and monovacant Keggin-type tungstophosphates are −12.9 and −10.4 ppm, respectively, which suggests that the Keggin unit in PW_{11}–SiO_2 tended to saturation due to grafting of organosiloxane units from the silica network to its vacant site. It must be noted that the IR vibration band of PW_{11}–SiO_2 at 1079 cm^{-1} may originate from a combination of the P–O bond in the central PO_4 and an Si–O–Si bond from the silica matrix.

Elemental analysis results show that the loadings of XW_{11} in the hybrid materials are relatively high, and the determined X : W ratio was *ca.* 1 : 11 for XW_{11}–SiO_2 composites (X = P, Ge, B), suggesting that the starting monovacant XW_{11} are stable during the process of TEOS hydrolysis and subsequent PS removal.

According to the above discussion we conclude that the primary XW_{11} structures remained intact after formation of the XW_{11}–silica hybrid materials. Both the observations that stretching and deformation vibration bands at the W–O–W bridge bonds of XW_{11} in the XW_{11}–SiO_2 composites are shifted to higher frequencies as compared with those of the starting XW_{11}, and that the ^{31}P chemical shift of PW_{11}–SiO_2 changes to a higher value compared to that of pure PW_{11} are attributed to saturation of the XW_{11} moiety through grafting of organosiloxane units. In this kind of composite, XW_{11} presents one vacant site, which allows the connection of two SiO_4 units from the silica network to make up one metal–oxygen octahedral lacuna. Therefore, the terminal nucleophilic oxygen atoms became bridge atoms due to connection of the electophilic silicon atom in the silanol unit *via* a W–O–Si bridge. The proposed representation of the structures of XW_{11}–SiO_2, based on the current work, is shown in Fig. 7. This model is also motivated by Thouvenot's work on this topic,[23–27] and they reported the synthesis of $[XW_9O_{34}(t\text{-}BuSiOH)_3]^{(8-n)-}$ and $[XW_9O_{34}(RSiO)_3(RSi)]^{(8-n)-}$ (R ≠ t-Bu) hybrids by reacting organosilane ($RSiCl_3$) with trivacant Keggin tungstate anions $[X^{n+}W_9O_{34}]^{(14-n)-}$ (X^{n+} = Si^{4+}, Ge^{4+}, P^{5+}, As^{5+}). In all these hybrid anions, three RSi groups acts as electrophile groups and are grafted onto the trivacant Keggin anion *via* six Si–O–W bridges, resulting in the saturation of the POM surface. They also reported that synthesis of $[\gamma\text{-}SiW_{10}O_{36}(RPO)_2]^{4-}$ *via* reaction of organophosphonic acids $RPO(OH)_2$ (R = H, Et, n-Bu, t-Bu, $C_2H_4CO_2H$, Ph) with the divacant anion $[\gamma\text{-}SiW_{10}O_{36}]^{8-}$, which also presents four nucleophilic surface oxygen atoms. The structures of the products were characterized by spectroscopic methods and by X-ray crystallography. That is, the hybrid anion is built up from a $[\gamma\text{-}SiW_{10}O_{36}]^{8-}$ unit and two electrophilic $PhPO^{2+}$ groups, which are linked to two oxygen atoms of two edge-shared WO_6 octahedra *via* a P–O–W bridge. Therefore, the product is fully saturated.

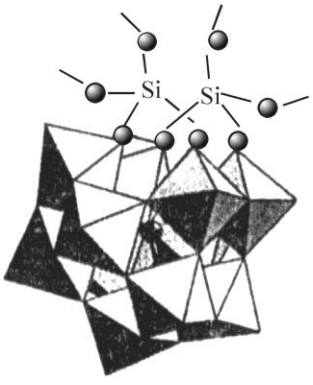

Fig. 7 Proposed representations of the structures of the SiW_{11}–SiO_2 composite. Each oxygen atom is represented by one black ball.

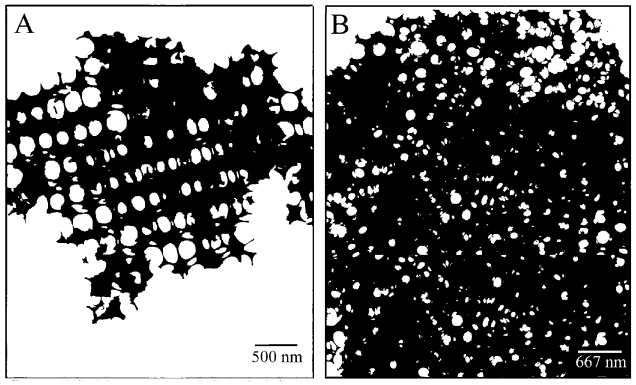

Fig. 8 TEM images of PW_{11}–SiO_2 with low (A) and high (B) magnification.

Macroporous structures of the XW_{11}–SiO_2 hybrid materials were formed as the PS template escaped, and the walls were composed of silica functionalized with XW_{11}. Both Stein and Pine have reported the mechanism of formation of the macroporous oxide materials in detail,[2,35] and the mechanism of formation of the macroporous POM materials is similar to that of the macroporous oxide materials. Here, SEM and TEM were used to assess the porous structure of the XW_{11}–SiO_2 materials, and the results are shown in Fig. 2 and 8. Fig. 2 shows the three-dimensional ordering of pores of XW_{11}–SiO_2 and some of the structural domains in the products are close packed. The average macropore diameter for the four composites is *ca.* 300 nm, and the wall thickness ranged from 55 to 100 nm (see Table 3). In general, the macropore diameter of as-synthesized composite should be equal to the diameter of the PS sphere (*ca.* 500 nm), however, the determined values are lower than the expected values, attributed to shrinkage of the structures during extraction of the PS template.[36,37] The wall thickness of the composite is related to the concentration of the inorganic precursor and hydrolysis time. From SEM images we also observed that some areas showed point defects although many of these regions were defect-free, and some PS spheres remained in the XW_{11}–SiO_2 materials although the majority of the PS was removed *via* extraction. The TEM image of PW_{11}–SiO_2 also shows that particles of PW_{11}–SiO_2 were well ordered (TEM image for the other three XW_{11}–SiO_2 composites were similar to that of PW_{11}–SiO_2). The walls of the hybrid silica materials correspond to dark areas, and the pores correspond to light areas.

In the case of the macroporous oxide materials, extraction or calcination of the PS template from the composite could produce macroporous structures with an amorphous wall, which in turn, exhibited micro- or meso-porous structures and high surface areas.[2] The porosity of the XW_{11}–SiO_2 wall was characterized by N_2 adsorption measurements. On account of structural similarity, the isotherms were represented by SiW_{11}–SiO_2 and PW_{11}–SiO_2 materials, respectively (Fig. 9), and BET surface areas are summarized in Table 3. The isotherms of PW_{11}–SiO_2 and SiW_{11}–SiO_2 are nearly reversible, therefore, we only provide the adsorption branch of the N_2 isotherms for PW_{11}–SiO_2 and SiW_{11}–SiO_2. According to the IUPAC definition, the isotherms belong to Type I. That is, the sharp increase in the adsorbed amount of N_2 at a very low relative pressure ($p/p_0 < 0.1$) occurred, indicating that the wall exhibited microporosity. The pore diameter is mainly distributed at *ca.* 1.0 nm for the above four composites. However, the pore volume for each of the XW_{11}–SiO_2 materials was smaller than that of the macroporous oxides reported, suggesting that only part of the micropores existed in the XW_{11}–SiO_2 wall. The low pore volume of the XW_{11}–SiO_2 wall may be due to crowding of the large Keggin units in the wall blocking part of the pores of the silica network. In comparison with pure XW_{11}, the surface

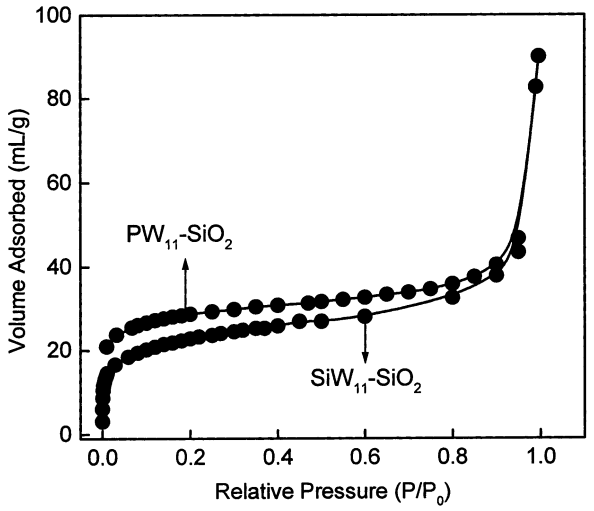

Fig. 9 Plots of nitrogen adsorption isotherms for PW_{11}–SiO_2 and SiW_{11}–SiO_2 composites.

areas of the composites have increased due to the formation of the porous materials.

3.3 Photocatalytic activity of the XW_{11}–SiO_2 composites

The intrinsic thermal redox and photoredox activities of polyoxometalates (POMs) are well known.[38–43] Up till now, much work has been done on studying POMs as heterogeneous thermal catalysts and applying them for industrial purposes. However, most studies on the photooxidative behavior of POMs have been with homogeneous solutions.[44,45] Preparation of heterogeneous POM photocatalytic materials in which the photocatalytic activity is comparable with the widely used semiconductor photocatalyst TiO_2 is of great interest because the support makes them easily handled and recycled.[46]

The present photocatalytic tests were run in air. On stirring the suspension of aqueous MA solution (100 mg l^{-1}) and XW_{11}–SiO_2 powder (containing 50 mg of pure XW_{11} in each XW_{11}–SiO_2 composite; X = P, Si, B) in the dark for 2 h the disappearance of MA was negligible. In the presence of macroporous SiO_2 (obtained under similar conditions to that of macroporous XW_{11}–SiO_2 except no inorganic precursor was added), *ca.* 12.9% of the MA disappeared under 2 h UV-irradiation. However, we observed apparent changes in the concentrations of MA by UV irradiation of the XW_{11}–SiO_2 suspension. Decreases in the MA concentration and changes in the concentrations of intermediates (acetic acid and formic acid) were analyzed simultaneously by IC, and the results are shown in Fig. 10. IC together with GC-MS also identified qualitatively 10 other intermediates such as hydroxyethanoic acid, tartaric acid, butenedioic acid, 2-oxopropanoic acid, oxalic acid, 1, 2-dihydroxypropanoic acid, propenoic acid, 2-hydroxypropanoic acid, acetaldehydic acid and propanedioic acid during the process of MA photodegradation on the XW_{11}–SiO_2 composites. However, only one intermediate (butenedioic acid) was detected under UV irradiation of the suspension of SiO_2 and MA under the same conditions. It indicates that degradation of MA mainly originated from photoexcitation of the XW_{11}–SiO_2 composites. The photocatalytic activity of POMs originates from their unique structure. UV irradiation of XW_{11} resulted in the formation of a $O \rightarrow W$ CT excited state $[XW_{11}]^*$ with considerable oxidizing capacity. Thus, XW_{11} which is otherwise thermally inactive for the degradation of aqueous MA becomes a powerful oxidant under the photoactivation by near-UV light. MA was totally degraded after *ca.* 160–180 min irradiation in the presence of XW_{11}–SiO_2. However, the intermediates were still observed by IC after MA totally disappeared. This suggests that mineralization of MA

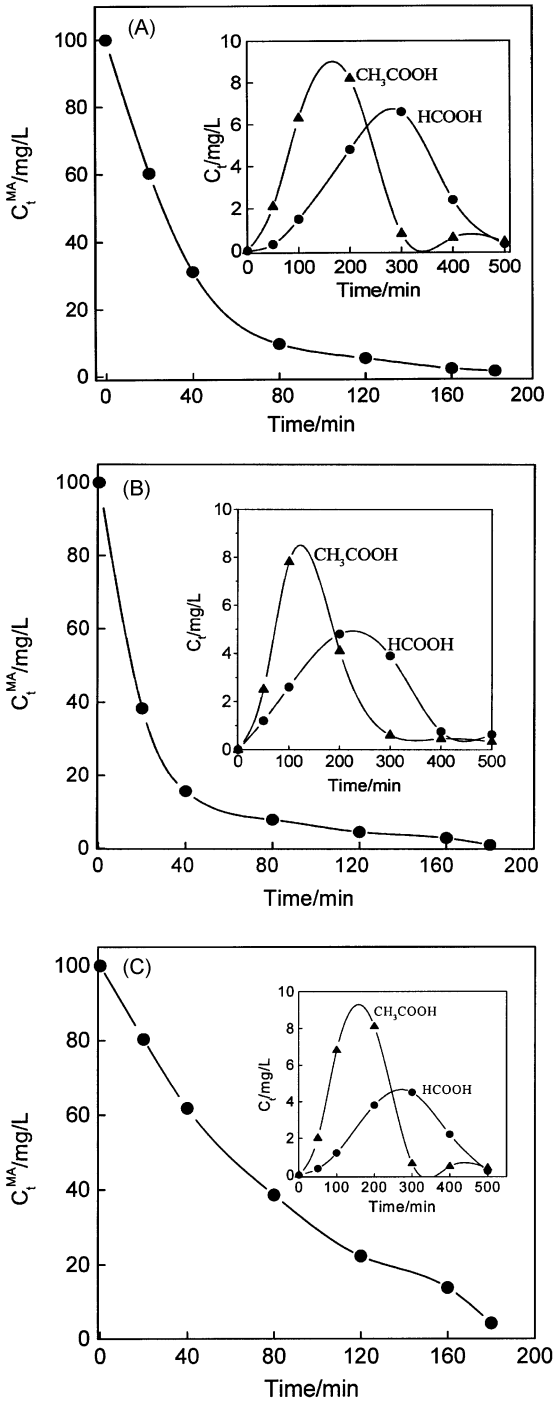

Fig. 10 Decreases in the MA concentration and changes in the acetic acid and formic acid concentrations during the UV irradiation of (A) PW_{11}–SiO_2, (B) SiW_{11}–SiO_2, and (C) BW_{11}–SiO_2. C_t^{MA} represents MA concentration at time t, and C_t represents acetic acid or formic acid concentration at time t.

required a reaction time longer than for degradation due to the successive carbon-chain degradation. After *ca.* 300 min irradiation, acetic acid disappeared. Formic acid disappeared completely after subsequent 120–200 min irradiation under the same conditions, indicating that mineralization of MA into CO_2 is complete after 420–500 min UV irradiation in the presence of the macroporous XW_{11}–SiO_2 composite.

ICP-AES analysis indicated that there was no leaching of W from the silica matrix into the reaction system during the catalytic tests, attributed to strong chemical interactions between organosilanol groups and the lacunary POM molecules in the composites. However, the leakage of catalyst often

occurs for the silica-supported porous solids prepared *via* conventional "impregnation" techniques.

4 Conclusions

A templating method of synthesis for three-dimensionally ordered macroporous $[X^{n+}W_{11}O_{39}]^{(12-n)-}$-silica (X = P, Si, Ge, B) composites is proposed. In order to obtain a well-ordered porous structure, the inorganic precursor, $[X^{n+}W_{11}O_{39}]^{(12-n)-}$, should have a high water-solubility, and the sizes of the PS template should be uniform. Characterization of the products confirms that the primary Keggin structures remain intact regardless of the functionality of the polyanions, and that the surface of the parent XW_{11} units tend to saturation through chemical grafting of organosilanol groups from the silica network. Investigation on the photocatalytic degradation of aqueous MA showed that XW_{11} retained photocatalytic activity in the hybrid materials.

Acknowledgements

The Natural Science Fund Council of China is acknowledged for financial support (no. 20071007). The present work is also supported by the Foundation for University Key Teacher by the Ministry of Education of China.

References

1 B. T. Holland, C. F. Blanford and A. Stein, *Science*, 1998, **281**, 538–540.
2 B. T. Holland, C. F. Blanford, T. Do and A. Stein, *Chem. Mater.*, 1999, **11**, 795–805.
3 J. E. G. J. Wijnhoven and W. L. Vos, *Science*, 1998, **281**, 802–804.
4 S. J. Sarrade, G. M. Rios and M. Carles, *Sep. Purif. Technol.*, 1998, **14**, 19–25.
5 A. Blanco, E. Chomski, S. Grabtchak, M. Ibisate, S. John, S. W. Leonard, C. Lopez, F. Meseguer, H. Miguez, J. P. Mondia, G. A. Ozin, O. Toader and H. M. Driel, *Nature*, 2000, **405**, 437–440.
6 B. T. Holland, L. Abrams and A. Stein, *J. Am. Chem. Soc.*, 1999, **121**, 4308–4309.
7 P. D. Yang, T. Deng, D. Y. Zhao, P. Y. Feng, D. Pine, B. F. Chmelka, G. M. Whitesides and G. D. Stucky, *Science*, 1998, **282**, 2244–2246.
8 H. Yan, C. F. Blanford, B. T. Holland, W. H. Smyrl and A. Stein, *Chem. Mater.*, 2000, **12**, 1134–1141.
9 R. A. Caruso, M. Giersig, F. Willig and M. Antonietti, *Langmuir*, 1998, **14**, 6333–6336.
10 A. Imhof and D. J. Pine, *Nature*, 1997, **389**, 948–951.
11 M. Antonietti, B. Berton, C. Göltner and H. P. Hentze, *Adv. Mater.*, 1998, **10**, 154–159.
12 S. A. Davis, S. L. Burkett, N. H. Mendelson and S. Mann, *Nature*, 1997, **385**, 420.
13 O. D. Velev, T. A. Jede, R. F. Lobo and A. M. Lenhoff, *Nature*, 1997, **389**, 447–448.
14 S. H. Park and Y. Xia, *Chem. Mater.*, 1998, **10**, 1745–1747.
15 C. R. Mayer and R. Thouvenot, *Chem. Mater.*, 2000, **2**, 257–260.
16 A. Imhof and D. J. Pine, *Adv. Mater.*, 1998, **10**, 697–700.
17 O. D. Velev, P. M. Tessier, A. M. Lenhoff and E. W. Kaler, *Nature*, 1999, **401**, 548.
18 P. Jiang, J. Cizeron, J. F. Bertone and V. L. Colvin, *J. Am. Chem. Soc.*, 1999, **121**, 7957–7958.
19 G. Subramania, K. Constant, R. Biswas, M. M. Sigalas and K.-M. Ho, *Appl. Phys. Lett.*, 1999, **74**, 3933–3935.
20 Y. A. Vlasov, N. Yao and D. J. Norris, *Adv. Mater.*, 1999, **11**, 165–169.
21 M. T. Pope and A. Müller, *Angew. Chem., Int. Ed. Engl.*, 1991, **30**, 34–48.
22 N. Mizuno and M. Misono, *Chem. Rev.*, 1998, **98**, 199–218.
23 N. Ammari, G. Herve and R. Thouvenot, *New. J. Chem.*, 1991, **15**, 607–611.
24 A. Mazeaud, N. Ammari, F. Robert and R. Thouvenot, *Angew. Chem., Int. Ed. Engl.*, 1996, **35**, 1961–1964.
25 C. R. Mayer and R. Thouvenot, *J. Chem. Soc., Dalton Trans.*, 1998, 7–13.
26 C. R. Mayer, P. Herson and R. Thouvenot, *Inorg. Chem.*, 1999, **38**, 6152–6158.
27 C. R. Mayer, I. Fournier and R. Thouvenot, *Chem. Eur. J.*, 2000, **6**, 105–110.
28 F. Xin and M. T. Pope, *Inorg. Chem.*, 1996, **35**, 1207–1213.
29 G.-S. Kim, K. S. Hagen and C. L. Hill, *Inorg. Chem.*, 1992, **31**, 5316–5324.
30 C. Brevard, R. Schimpf, G. Tourne and C. M. Tourne, *J. Am. Chem. Soc.*, 1983, **105**, 7059–7063.
31 N. Haraguchi, Y. Okaue, T. Isobe and Y. Matsuda, *Inorg. Chem.*, 1994, **33**, 1015–1020.
32 Y. Guo, Y. Wang, C. Hu and E. Wang, *Chem. Mater.*, 2000, **12**, 3501–3508.
33 Y. Guo, D. Li, C. Hu, Y. Wang and E. Wang, *Appl. Catal. B*, 2001, **3-4**, 337–349.
34 M. T. Pope, *Heteropoly and Isopoly Oxometalates*; Springer Verlag: Berlin, 1983.
35 G. Subramanian, V. N. Manoharan, J. D. Thorne and D. J. Pine, *Adv. Mater.*, 1999, **11**, 1261–1265.
36 A. Stein, M. Fendorf, T. P. Jarvie, K. T. Mueller, A. J. Benesi and T. E. Mallouk, *Chem. Mater.*, 1995, **7**, 304–313.
37 O. D. Velev, T. A. Jede, R. F. Lobo and A. M. Lenhoff, *Chem. Mater.*, 1998, **10**, 3597–3602.
38 I. V. Kozhevnikov, *Chem. Rev.*, 1998, **98**, 171–198.
39 T. Okuhara, T. Nishimura and M. Misono, *Stud. Surf. Sci. Catal.*, 1996, **101**, 581–588.
40 N. Mizuno and M. Misono, *Chem. Rev.*, 1998, **98**, 199–217.
41 R. F. Renneke and C. L. Hill, *J. Am. Chem. Soc.*, 1990, **112**, 6585–6594.
42 T. Yamase, N. Takabayashi and M. Kaji, *J. Chem. Soc., Dalton Trans.*, 1984, 793–799.
43 H. Einaga and M. Misono, *Bull. Chem. Soc. Jpn.*, 1997, **70**, 1551–1557.
44 A. Mylonas and E. Papaconstanitinou, *J. Photochem. Photobiol. A*, 1996, **94**, 77–82.
45 I. Texier, C. Giannotti, S. Malato, C. Richter and J. Delaire, *Catal. Today*, 1999, **54**, 297–307.
46 D. A. Friesen, J. V. Headley and C. H. Langford, *Environ. Sci. Technol.*, 1999, **33**, 3193–3198.